Droplet Characteristics in a Countercurrent Contactor

R. B. OLNEY

Shell Development Company, Emeryville, California

There are a number of countercurrent flow devices used in liquid-liquid extraction studies in which the dispersed phase exists as discrete drops. Examples include spray and perforated plate columns and rotating-disk, rotating-impeller, and rotating-cylinder contactors. In order to achieve a useful analysis of extraction data from such devices, the assumption commonly is made that the drops are spherical and of uniform size. This permits one to then define an interfacial area $\bar{a}$, contact time $\bar{t}$, and transfer coefficient $\bar{k}$ based on the average drop, from which is obtained the characteristic number of transfer units $\bar{T} = \bar{K}\bar{a}\bar{t}$ at a certain plane in contactor space and for the drop population as a whole.

However, it is well known that disperser or inlet feed devices commonly used in extraction columns form rather wide distributions of drop sizes. Examples which show this tendency include investigations with spray columns (*7*), orifice dispersers (*15*), stirred vessels (*6, 13, 14*) and rotating cylinder apparatus (*1*). Moreover, beyond the inlet there are the competing effects of generation of new drops due to shear or local turbulence in the bulk flow, and of droplet coalescence due to drop interaction effects (*9, 10*). Depending upon the characteristics of the particular flow contactor there will then be a balance among these several processes such that, at a distance considerably removed from the inlet, two limiting situations may be visualized: a distribution of drop sizes and drop residence times (little drop interaction), or a size distribution of drops all essentially of the same age (equal probability of repeated coalescence and redispersion among drops of all sizes). This size distribution may be considered to be bounded by an upper limit or maximum stable size (*3, 17*) and a lower limit or minimum size, depending upon the break-up processes prevailing. Moreover, this minimum size, as viewed at a fixed station by an observer, may be dictated by the size that is just entrained by the counterflowing continuous phase. In the simplest analysis, the age distribution just mentioned is given directly, in the absence of coalescence effects, by the hindered settling rates of the size fractions present.

Extending the noncoalescing drop picture one step further to include axial mixing effects in the contactor, the large drops which are present escape or bypass much more rapidly through the contact zone than does the average drop, whereas the smallest drops persist for long times and may be highly backmixed, owing to their small inertia by any gross eddy motions in the continuous phase. If mass transfer is occurring between the phases, then the above several effects lead to a transfer process that is not described, except fortuitously, by the usual simplified transfer mechanism based on the volume-surface mean diameter drop. Differences between the real and idealized situations will depend upon the particular transfer mechanism between drops and continuous phase and may be particularly acute for high-purity extractions or when backmixing is severe.

One purpose of the study described here is to present an interpretation of drop size distribution data obtained in a contactor for which a fairly complete analysis of drop dynamics and mass transfer processes based on the simplified (average drop) concept has already been published (*18*). In this way one is better able to judge the condi-

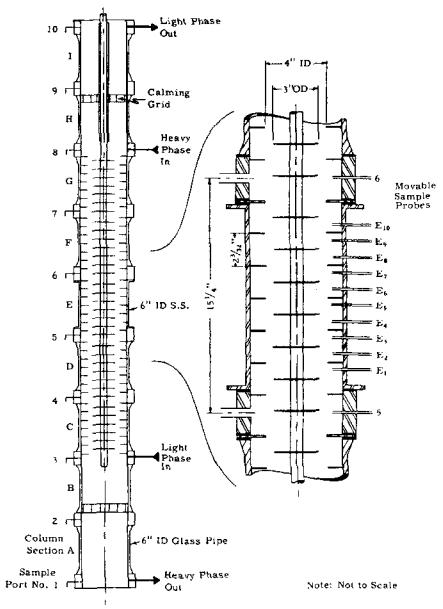

Fig. 1. Sketch of RDC 34-6/4/3-2.1. Dimensions in inches.

TABLE 1. SYSTEMS USED IN DROP SIZE DISTRIBUTION STUDY

Dispersed phase	Continuous phase	g./cc. ρ_C	g./cc. ρ_D	centipoise μ_C	centipoise μ_D	σ, dyne/cm.	N, rev./min.	ft./hr. V_C	ft./hr. V_D	Drop holdup, h	θ,* sec.
Toluene	Water	1.0	0.87	1.13	0.61	34	350	21.4	21.4	0.04	33.7
							550	17.1	17.1	0.08	84.3
							650	10.7	10.7	0.12	202
							650	12.8	12.8	0.15	211
							650	21.4	21.4	0.38	320
Toluene	60% Glycerol	1.141	0.863	9.1	0.58	26	350	12.8	12.8	0.14	197
							450	8.6	8.6	0.17	376
White oil	Water	0.998	0.867	1.0	26.0	50	650	42.8	42.8	0.14	58.9
							800	30.0	30.0	0.15	90.1
							1100	8.6	8.6	0.13	272
68% Kerosene 32% CCl_4	Water	0.998	1.053	1.05	1.44	43	400	25.7	25.7	0.11	77.1
							550	15.0	15.0	0.10	120
							700	7.5	7.5	0.11	264
37% Kerosene 63% CCl_4	Water	1.0	1.30	1.05	1.17	41	600	55.6	55.6	0.12	38.9
							800	34.2	34.2	0.12	63.2

* Average drop residence time in test section, $\theta = hL/V_D$.

tions under which the assumption of uniform drop size may lead to serious error, when interpreting mass transfer and related processes in discrete-drop apparatus. A second purpose is to outline the general features of the problem covering mass transfer between a continuous phase and an assemblage of drops of all sizes, when accompanied by axial diffusion of each phase. Numerical solution of the equations governing this case has not been attempted; however, it is possible to point out, just from inspection of these equations, certain situations wherein the uniform-drop model may be significantly in error.

EXPERIMENTAL METHODS

The photographic study was done in a 6-in. diameter rotating disk contactor (RDC); the principal features and dimensions of the unit are shown in Figure 1. Performance data for this and other RDC's were presented in an earlier paper (*18*). The column was operated with continuous recycle of both liquid phases under countercurrent flow conditions. Several flow rates and RDC rotor speeds were used with each liquid pair studied. Photographs were taken at a station twenty-three or twenty-four compartments removed from the dispersed-phase inlet. This distance from the inlet corresponds to drop residence times (average) of 0.4 to 19 min. in the contact zone, depending upon the holdup and flow rate of the dispersed phase. It is not known if equilibrium maximum drop sizes or size distributions were attained in this distance of travel; however, photography at greater distances from the inlet could not be done conveniently in the present study. The liquid systems were equilibrated by recycling through the column for an extended period before photographs were taken. Drop holdups were measured in the vicinity of the region photographed, with the sample probes illustrated in Figure 1.

An exposure time of ~0.001 sec. was used, which served to produce comparatively sharp drop outlines at all rotor speeds. Photographs were taken through the glass wall of the column, and the area photographed was about 2.3 in. high (bracketing one compartment) and 2 in. wide. This width is only about 10% of the column periphery, and distortion due to curvature is therefore not very important. The camera was focused to give sharp images of the central field, so the depth of the field (distance in from column wall) was greatest, perhaps 1 in., for large drops and low holdups and was least for very small drops and high holdups. Replicate photographs, usually four or six, were taken of each event studied. Drop sizes were determined from ~4X enlargements from the original negatives. Typical drop photographs for one of the liquid systems, at four different rotor speeds, are given in Figure 2.*

Maximum stable drop size data for nine liquid-liquid pairs were reported earlier (*18*). The same photographs from which d_m was determined were available for the present size distribution analysis. However, certain of the systems (especially at higher rotor speeds) yielded photographs that did not permit determining the size and number of the smaller drops present. Also, all of the photographs for systems with aqueous phase dispersed were too clouded by the presence of extremely small drops to permit making reliable drop counts. There remained photographs for a total of fifteen runs with five liquid pairs (organic phase dispersed) which gave satisfactory data. The properties of these liquid systems and the run conditions are given in Table 1, and the size distribution data are discussed in the next section. Drop counts were made from two or three replicate photographs for most of the runs, in order to determine the reliability and precision. Illustrative data from replicate determinations are given in Table 2.* The size range on each photograph was divided into a number of intervals (for example, see Table 2), and the drop count in each interval was determined by means of a pair of dividers. As in the previous study (*18*) highly distorted drops (which were few in number) were neglected; in general, the drops counted had a major/minor axes ratio of less than 1.3.

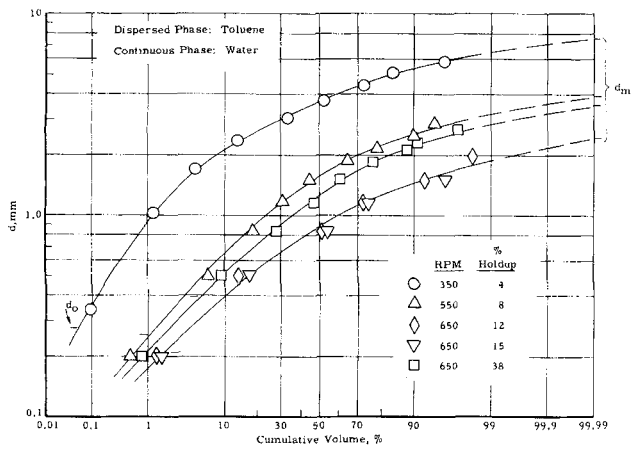

Fig. 3. Drop size distributions, 6-in. RDC.

SIZE DISTRIBUTION DATA

Drop size-cumulative volume curves are shown in Figures 3 through 7 for the five systems. The maximum drop size determined from the same photograph is shown for

* Tabular material and Figure 2 have been deposited as document 8089 with the American Documentation Institute, Photoduplication Service, Library of Congress, Washington, 25, D. C., and may be obtained for $1.25 for photoprints or 35-mm. microfilm.

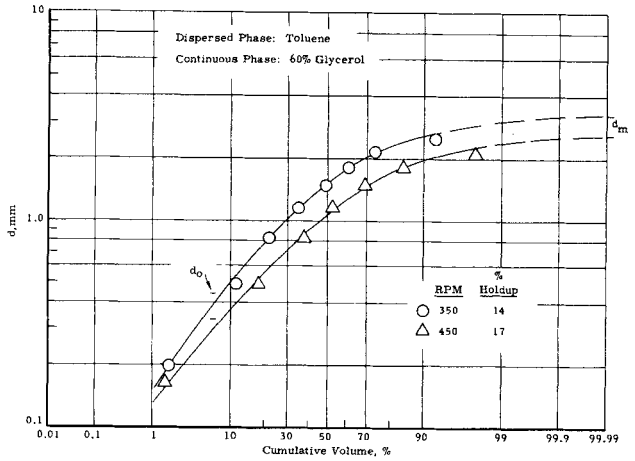

Fig. 4. Drop size distributions, 6-in. RDC.

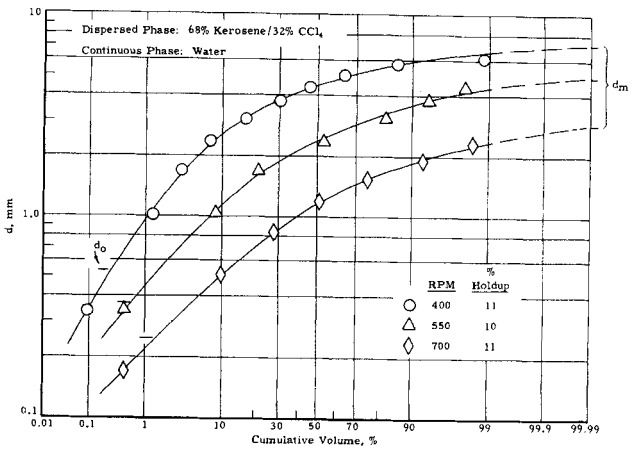

Fig. 6. Drop size distributions, 6-in. RDC.

each run on the right-hand vertical scale of the figure. The variables studied include rotor speeds between 350 and 1,100 rev./min. and drop holdups between 4 and 38%, as well as the properties ρ_c, ρ_d, μ_c, μ_d, and σ shown in Table 1. As will be shown in more detail later, several of these variables, especially rotor speed, have a marked effect on the average or characteristic drop size but not much effect on the parameters of the size distributions. As one example, the data for white oil dispersed in water (Figure 5) show that the volume-median drop size d_{50} decreases from 3.1 to 0.8 mm. as rotor speed is increased from 650 to 1,100 rev./min., but the width of the size distribution, as described by d_{95}/d_5, changes only from 4.5 to 4.2.

Curves which show the effect of drop concentration (holdup) on the size distribution at a given rotor speed are included in Figure 3 (runs at 650 rev./min. and h = 0.12, 0.15, and 0.38). The increase in drop sizes over the whole spectrum, as holdup is increased, may be caused solely by higher drop interaction rates due to smaller interparticle distances. On the other hand, the specific power input (power/mass of dispersed phase = $\rho N^3 R^5/\rho_d h\, HD^2$) may also be a factor in the dispersion process.

Several parameters of the size distributions are tabulated in Table 3. These include d_{50} and the ratios d_{32}/d_{50}, d_{95}/d_{50}, and d_5/d_{50}. More will be said later about the ratios d_{95}/d_{50} and d_5/d_{50} as well as the uniformity and skewness parameters δ and a. The volume-surface (Sauter) mean diameter d_{32} is calculated as

$$d_{32} = \frac{\Sigma n_i d_i^3}{\Sigma n_i d_i^2} \qquad (1)$$

It is seen that d_{32}/d_{50} ranges from 0.79 to 1.06; Mugele (*11, 12*) outlines the range of d_{32}/d_{50} to be expected for certain types of sprays and dispersions.

It is of interest to compare the experimental d_{32} values determined from the drop photographs with the d_{32} calculated via the methods outlined in the previous study (*18*), namely

$$d = fn\,(u, \rho_c, \Delta\rho, \mu_c, \sigma) \quad \text{[Terminal velocity curve, obtained from work of (4, 5, 8)]} \qquad (2)$$

where $d_{32} = d$ when $u = \bar{u}$, $\bar{u}$ being defined by Equations (3) and (4):

$$\bar{u} = \frac{1}{C_R(1-h)}\left[\frac{V_d}{h} + \frac{V_c}{1-h}\right] \qquad (3)$$

$$C_R = \text{minimum of} \begin{cases} 1-(R/D)^2 & (4a) \\ (S/D)^2 & (4b) \\ \left(\dfrac{S+R}{D}\right)\sqrt{\left(\dfrac{S-R}{D}\right)^2 + \left(\dfrac{H}{D}\right)^2} & (4c) \end{cases}$$

The minimum constriction factor C_R is ~0.45 for the 6-in. RDC, and h is the experimental value of the drop holdup. Values of d_{32} so calculated are compared with the experimental values for the five liquid systems in Figure 8. The agreement is quite good, the average deviation from the 45-deg. line being 10.5%. This indicates that the velocity relations for the uniform drop, given by Equations (2), (3), and (4), apply well to the average of a swarm of drops in an RDC.

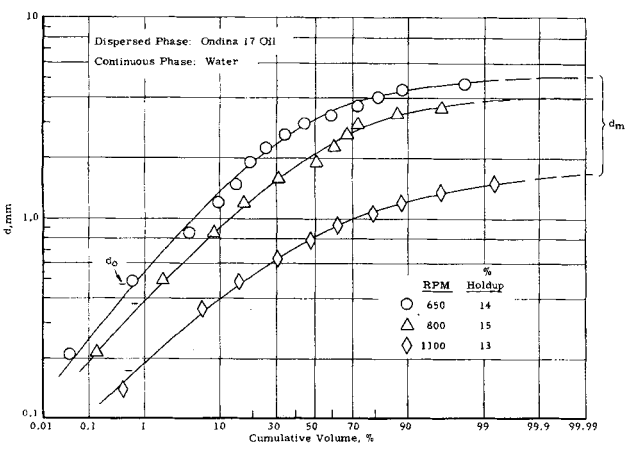

Fig. 5. Drop size distributions, 6-in. RDC.

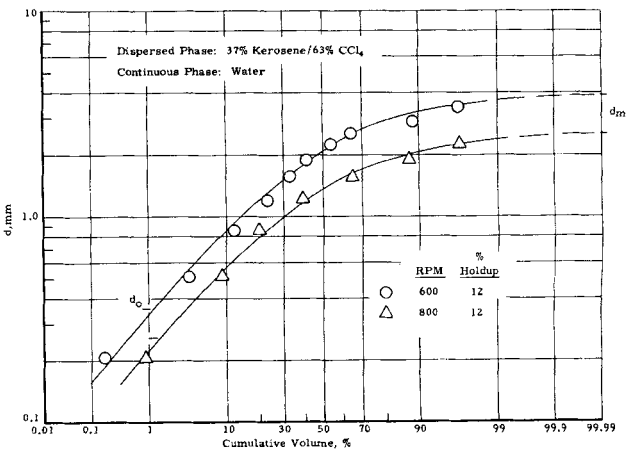

Fig. 7. Drop size distributions, 6-in. RDC.

TABLE 3. PARAMETERS OF SIZE DISTRIBUTION CURVES

Dispersed phase	Continuous phase	N, rev./min.	Drop holdup, h	d_{50}, mm.	d_{32}/d_{50}	d_{95}/d_{50}	d_5/d_{50}	d_{32} from size distribution, mm.	d_{32}, calculated,* mm.	Upper-limit distribution parameters δ	a
Toluene	Water	350	0.04	3.6	0.98	1.60	0.47	3.54	4.17	0.94	1.03
		550	0.08	1.5	0.89	1.85	0.31	1.34	1.71	0.79	1.59
		650	0.12	0.82	1.06	2.08	0.39	0.89	0.86	0.88	1.64
		650	0.15	0.83	1.01	1.81	0.35	0.85	0.86	0.89	1.96
		650	0.38	1.21	0.94	2.06	0.32	1.14	1.05	0.78	1.91
Toluene	60% Glycerol	350	0.14	1.5	0.79	1.80	0.22	1.19	1.38	0.60	1.20
		450	0.17	0.95	0.90	1.98	0.26	0.95	0.99	0.70	1.50
White oil	Water	650	0.14	3.0	0.82	1.50	0.33	2.49	2.70	0.66	0.67
		800	0.15	2.0	0.87	1.68	0.32	1.80	1.77	0.69	0.88
		1100	0.13	0.80	0.93	1.63	0.39	0.75	0.64	0.83	1.07
68% Kerosene 32% CCl_4	Water	400	0.11	4.5	0.91	1.33	0.43	4.10	3.46	1.04	0.62
		550	0.10	2.2	~1.0	1.77	0.38	2.25	2.18	0.81	1.18
		700	0.11	1.15	0.96	1.71	0.33	1.10	1.08	0.85	1.59
37% Kerosene 63% CCl_4	Water	600	0.12	2.1	0.83	1.66	0.30	1.69	2.30	0.68	0.95
		800	0.12	1.35	0.89	1.56	0.30	1.20	1.39	0.72	0.97

* Calculated via Equations (2), (3), and (4), and with measured values of h used.

The fact that one can predict the characteristic settling diameter for a drop population from single-drop dynamics does not mean that this diameter suitably represents all events of interest in a countercurrent-flow device, however. To illustrate, suppose that there is a distribution of sizes present, such that the fraction of drops f_i has a diameter d_i, slip velocity u_i, and contact time $t_i = L/u_{di}$, where u_{di} is given by

$$u_{di} = u_i C_R (1-h) - \frac{V_c}{1-h} \qquad (3a)$$

The appropriate drop diameter that represents the average transfer rate for a mass transfer process will then depend upon the transfer mechanism and the parameters of the size distribution, and this diameter will not necessarily be d_{32}. For example, one might encounter the simple situation where the transfer rate for fraction f_i is limited by molecular diffusion in drops, such that the first-term approximation of the Newman equation applies:

$$\frac{(k_D a)_i t_i}{h} \cong 4\pi^2 \frac{\mathcal{D}_D t_i}{d_i^2} \text{ giving} (k_D)_i \sim d_i^{-1} \qquad (5)$$

Or it may be that transfer in circulating-oscillating drops is the limiting mechanism, for which (2)

$$\frac{(k_D a)_i t_i}{h} \cong 0.0225 \frac{u_i t_i / d_i}{\left(1 + \frac{\mu_d}{\mu_c}\right)} \text{ giving } (k_D)_i \sim u_i \qquad (6)$$

Or it may be that an outside-film resistance limits the transfer rate, such that a film penetration or surface renewal model applies:

$$\frac{(k_c a)_i t_i}{h} = 6\sqrt{\frac{4}{\pi}} \sqrt{\frac{\mathcal{D}_c u_i}{d_i}} \frac{t_i}{d_i} \text{ giving}$$

$$(k_c)_i \sim \sqrt{\frac{u_i}{d_i}} \qquad (6a)$$

(In all cases one assumes that area $a_i = 6h/d_i$.) Whichever equation applies in a particular case, it must be summed over the range of drop sizes present to give the average transfer rate. But the grade-fraction values of u_i and t_i are not linear functions of the d_i's, and so the average $\bar{d}$ that represents the transfer rate for the total drop population is not likely to be d_{32}. Addition of axial diffusion effects for the drop phase and continuous phase complicates still further the matter of the proper average diameter to use to represent the average transfer rate. Some discussion of this general case is given later.

As an illustrative example, numerical calculations which show that d_{32} does not give the average transfer rate are given in Table 4* for the molecular diffusion model [infinite series form of Equation (5)] and use the drop size distribution obtained for oil dispersed in water (Figure 5 at 1,100 rev./min.). For the conditions listed, it is seen that the uniform drop calculation gives 87.0% extraction of solute, while the size distribution calculation, summed over twelve size intervals, corresponds to only 76.7% extracted. It is not intended here to convey the thought that this simplified procedure applies to a practical extraction, and in any event it is likely that more than one transfer mechanism would enter into a dominant role over a wide spectrum of drop sizes. Nevertheless, the illustration serves to emphasize the sort of error that arises when one applies uniform-drop assumptions to drop populations.

For these reasons a further analysis of the size distribution data has been made. It is shown in the next section that the data obey the upper limit distribution proposed by Mugele and Evans (11), and, accordingly, the experi-

* See footnote on p. 828.

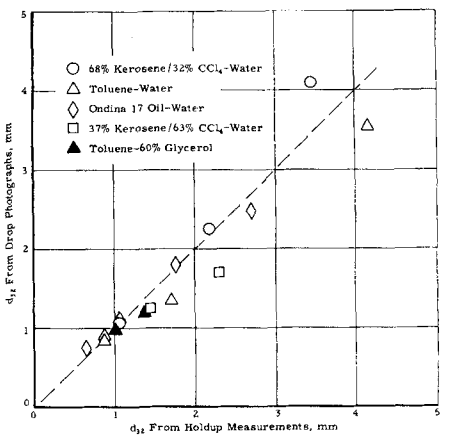

Fig. 8. Sauter mean diameters, 6-in. RDC.

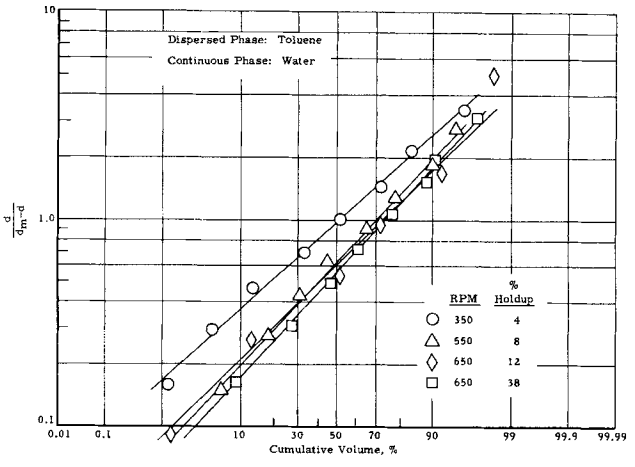

Fig. 9. Upper limit distribution, 6-in. RDC.

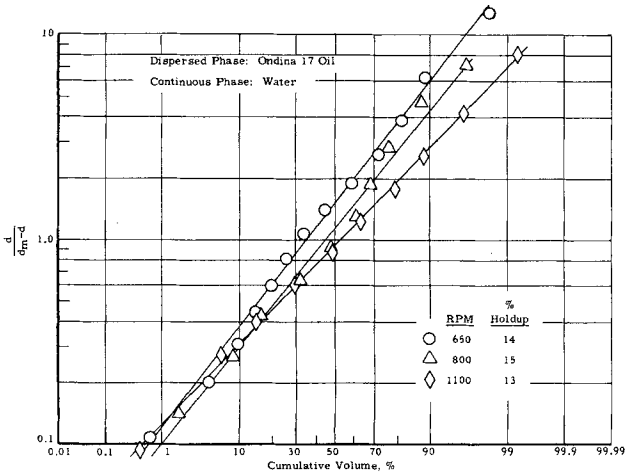

Fig. 10. Upper limit distribution, 6-in. RDC.

mental distributions can be characterized rather well in terms of the uniformity and skewness parameters δ and a given by them.

UPPER LIMIT DISTRIBUTION CORRELATION

Mugele and Evans (*11*) have proposed an upper limit distribution (ULD) defined in terms of a maximum particle size. This view is also in accord with the concepts of a maximum stable drop size in a turbulence or in shear flow, as discussed by Hinze (*13*), Sleicher (*17*), and others, and as demonstrated experimentally for the RDC in earlier work (*18*). The special upper limit function, as applied to log-probability distributions, is given by

$$\frac{dv}{dy} = \frac{\delta}{\sqrt{\pi}} e^{-\delta^2 y^2} \tag{7}$$

where

$$y = \ln\left(\frac{ad}{d_m - d}\right) \tag{8}$$

From a straight-line plot of $(d/d_m - d)$ vs. v on log-probability paper one obtains

$$a = \text{skewness parameter} = \frac{d_m - d_{50}}{d_{50}} \tag{9}$$

$$\delta = \text{uniformity parameter} = \frac{0.907}{\ln_e\left(\frac{d_{90}}{d_m - d_{90}} \cdot \frac{d_m - d_{50}}{d_{50}}\right)} \tag{10}$$

Size distribution data for two of the liquid systems are shown in terms of the upper limit function in Figures 9 and 10. The value of d_m used in each run is the maximum stable drop size observed on that particular photograph (see Table 2* for example calculation); the number of drops of size d_m used in the calculation is given by

$$n_m \frac{A_c}{A_t} \tag{11}$$

where

n_m = number of drops of size d_m on entire photograph (generally one)
A_t = area of entire photograph
A_c = area of portion of photograph on which drop-size count was made

Quite good upper limit plots were obtained for the other three liquid systems as well. The parameters δ and a, determined for the five liquid systems, are tabulated in Table 3. The index δ determines the spread of the distribution, a smaller value indicating a wider range of drop sizes, while a value of a greater than unity indicates a wider range of drops of sizes larger than d_{50}. The range of the uniformity parameter δ for the present data is 0.60 to 1.04; this compares, for example, with a range of 0.60 to 1.5 tabulated by Mugele (*12*) for pressure and tangential nozzles and rotating-cup, whirl-chamber, and venturi atomizers.

The question of a minimum drop size d_o is also of practical consequence for countercurrent-flow conditions, since Equation (3*a*) shows that drops of sufficiently small size will be entrained by the continuous phase ($u_d < 0$). Of course, eddy diffusion and drop redispersion will tend to cause some very fine drops to be present at the photographic station in any event. Nevertheless, the d_o corresponding to $u_d = 0$ in Equation (3*a*) should be in rough agreement with the smallest drops observed in the photographs. The small horizontal tics shown beside each curve in Figure 3 through 7, are the calculated d_o corresponding to $u_d = 0$ for each run condition. The agreement with the smallest observed drops is fair, poorest agreement occurring when the continuous phase is viscous (toluene dispersed in 60% glycerine).

COMPARISON WITH OTHER LIQUID-LIQUID DISPERSION DATA

The size distribution data for liquid-liquid dispersions obtained by Clay (*1*) in an 82 × 50 mm. rotating cylinder apparatus and in a 4-in. diameter circulating pipe loop are perhaps the best available ones with which comparisons can be made. Clay reported only the 10, 50, and 95% diameters, and so the author's data and the Clay data will be compared in those terms. Data for representative liquid systems from the Clay experiments and from this work are given in Table 5.* The rotating cylinder data cover a wide range of viscosities and interfacial tensions. The velocity tabulated is the inner cylinder speed for the cylinder apparatus and disk speed for the RDC and flow velocity for the pipe apparatus. Drop contact time is the total time for the batch experiments done by Clay and is the average drop rise time in the RDC flow experiments. The pump used by Clay in the pipe loop studies probably determined the drop size characteristics in that apparatus, and so the pipe data should not be given much weight.

The three devices listed in Table 5* give size distributions that are roughly similar, although changes in rotor speed or pipe velocity, drop concentration, contact time, and other variables apparently cause some changes in the d_{95}/d_{50} and d_{10}/d_{50} ratios. The reasons for these similari-

* See footnote on p. 828.

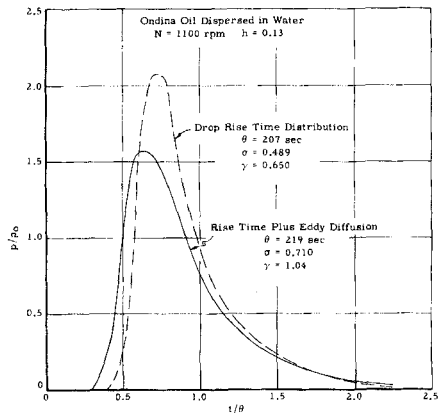

Fig. 11. Calculated distribution of drop residence times.

ties and differences cannot be isolated until such time as mechanisms for drop break up and drop interaction are known. Various speculations as to break-up mechanisms have been published (for example, reference 3); these, however, do not explain the existence of the wide distributions found in practice under the dynamic conditions of coalescence and break up. A problem of particular difficulty is that of explaining the formation of the many small drops found in a drop population and the persistence of these small drops (when present among drops of all sizes) when drop interaction rates are high.

DISTRIBUTION OF DROP RISE TIMES

For the interpretation of drop behavior given in this and subsequent sections one assumes that the drops, once formed, do not coalesce during their rise period in the contact zone. Repeated coalescence and break up of the drop population would, of course, alter the interpretation. The problem of drop interaction cannot yet be handled, however, since nothing is known about the relative probabilities of interaction of drops of different sizes in a dynamic environment.

The distribution of drop sizes observed in a countercurrent-flow extractor corresponds to a distribution of drop rise velocities and, in a given length of column, to a certain distribution of rise times. The spread of drop rise times may be greater than or less than the spread of drop sizes, depending upon whether the drops are small (Stokes settling, $u \sim d^2$) or large (constant drag coefficient, $u \sim \sqrt{d}$). Since the size range at typical operating conditions may extend from nearly Stokes conditions to well into the intermediate settling region, this means that the rise-time distribution will be highly skewed. The front end of the rise-time curve (large drops, short times) ascends very steeply, beginning at a finite time corresponding to d_m, while the tail of the curve extends out to the very long residence times of drops of size $\approx d_o$. Moreover, each fraction of the size distribution as seen by the observer (camera) must be multiplied by the velocity u_{di} corresponding to that size d_i to give the fraction of drops originating from the inlet feed which has a rise time t_i.

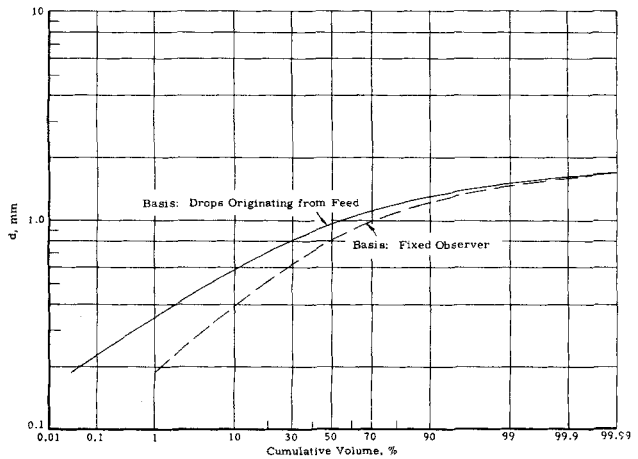

Fig. 12. Typical size distribution calculation.

A rise time distribution plot which illustrates these affects is given in Figure 11 (dashed curve), where the size distribution is that for the run with oil dispersed in water at 1,100 rev./min. (Figure 5), and the rise time distribution is calculated in the following manner. The size distribution curve is divided into p size fractions covering the range $d_{\min}$ to $d_{\max}$, and for each d the corresponding u from Equation (2) and u_d from Equation (3a) are determined. The fraction f_i, seen fixed in space on the photograph, is actually moving at a velocity u_{di}; therefore, the fraction of drops of this size that originates from the feed is given by

$$g_i = f_i u_{di} \Big/ \sum_{d_i=d_{\min}}^{d_i=d_{\max}} f_i u_{di} \qquad (12)$$

The two size distribution curves $f = fn(d)$ and $g = fn(d)$ for the run referred to are plotted on a cumulative volume basis in Figure 12. For a given column length, g_i is the fraction of feed rising in a time $t_i = L/u_{di}$. Therefore $\Delta g_i/\Delta t_i$ is proportional to $p(t_i)$, where $p(t_i)$ is the probability that the rise time will be between t_h and t_i, and where $\Delta t_i = t_i - t_h$. The properties of the rise time distributions are determined from the zero, first, second, and third moments of the probability curves so constructed; that is

$$p_o = \int p\, dt \qquad (13)$$

$$\theta = \frac{1}{p_o} \int t\, p\, dt \qquad (14)$$

$$\sigma^2 + 1 = \frac{1}{p_o \theta^2} \int t^2\, p\, dt \qquad (15)$$

$$\gamma^3 + 3\sigma^2 + 1 = \frac{1}{p_o \theta^3} \int t^3\, p\, dt \qquad (16)$$

In each case the limits of (numerical) integration are $t = t_{\min}$ ($d = d_{\max}$) to $t \to \infty$ ($u_d \cong 0$). p/p_o is given as a function of t/θ in Figure 11.

JOINT DISTRIBUTION, RISE TIME PLUS EDDY DIFFUSION

Eddy diffusion in a countercurrent-flow device will also affect the holding time distribution of the drop phase. Backmixing experiments in several sizes of RDC's with the continuous phase alone have already shown (*18*) that a correlation of VH/E_b and RN/V is obtained, of the general form

$$\frac{E_b}{VH} = b_o + b_1 Z \left(\frac{RN}{V}\right) \qquad (17)$$

where Z is a function of the geometry ratios S/D, R/D, H/D. One might expect, as a first approximation, a similar correlation of droplet eddy diffusivities if the drop velocity u_d is substituted for V. Some confirmation is provided by the particle eddy diffusivities obtained in a few settling tests with two narrow size fractions of solid particles (*18*); these data indicate that the E_b for the particles is about 40% greater than the E_b determined for single-liquid flow in the 6-in. RDC. For purposes of illustration here, one will make the assumption that $(E_b)_{\text{drop}} \cong (E_b)_{\text{cont phase}}$, and the equation, specific for the 6-in. RDC, then becomes

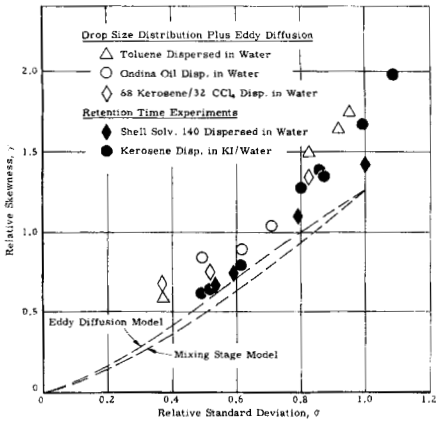

Fig. 13. Standard deviation, skewness relations.

$$\frac{E_b}{u_d H} \cong 0.2 + 0.004\left(\frac{RN}{u_d}\right) \tag{18}$$

The overall Peclet number for the drop fraction f_i of size d_i and velocity u_{di} is given by

$$N_{PeDi} = \frac{u_{di}L}{E_b} = \frac{u_{di}H}{E_b}\frac{L}{H} \tag{19}$$

The manner in which the joint distribution (that due to rise time plus eddy diffusion) is calculated involves operating on each size fraction with an appropriate eddy diffusion mechanism, then summing over all size fractions and all times. The eddy diffusion equation used is that for an infinite strip; for the i^{th} size fraction this equation is

$$C_i = \frac{f_i}{\sqrt{4\pi}}\sqrt{\frac{N_{PeDi}}{\lambda_i}} \exp\left[-\left(\frac{N_{PeDi}}{4}\right)\left(\sqrt{\lambda_i} - \sqrt{\frac{1}{\lambda_i}}\right)^2\right] \tag{20}$$

where $\lambda_i = v/t_i$ with v being a new time variable, not to be confused with the characteristic time t_i. The C's are calculated for all fractions and are plotted as functions of v, giving a family of curves with the t_i's as parameter. Sufficient time increments $\Delta v_1, \Delta v_2, \ldots\ldots$ are selected so as to span the time domain, and for each increment Δv the function $p(v)$ is determined:

$$p(v_n) = \frac{1}{\Delta v_n}\frac{\sum_{d_i=d_{\max}}^{d_{\min}} C_i \Delta\lambda_{in}}{\sum_{v_n=0}^{\infty}\sum_{d_i=d_{\max}}^{d_{\min}} C_i \Delta\lambda_{in}} \tag{21}$$

where $\Delta\lambda_{in} = \Delta v_n t_i$ and $\Delta v_n = v_n - v_m$. As in the previous section, the distribution function $p(v)$ so constructed is normalized, and the properties θ, σ, and γ are determined from the first, second, and third moments of the curves. Here, however, the limits of integration are $v = 0$ to $v = \infty$.

An example of a residence time distribution curve so calculated is shown in Figure 11 (solid curve) for the run with white oil dispersed in water at 1,100 rev./min. Values of θ, σ, and γ from the joint distribution model for ten of the runs (three liquid pairs) from the present study are given in Table 6.* It is seen that σ lies between 0.37 and 0.95, and γ is between 0.58 and 1.74. These values show that the spread of the calculated distribution curves is quite large, increasing with rotor speed, and that the leading edge of the curves rises sharply at early times. The θ from first moment calculations (Table 6*) may be compared with those calculated from average properties (Table 1).

The calculated curves for the joint distribution model may be compared with experimental curves obtained in drop phase retention time distribution tests done in the same 6-in. RDC. In these tests a pulse of tracer (insoluble in continuous phase) is introduced with the entering drop phase at time = 0, and the output of tracer concentration is determined as a function of time. Two sets of such data are available, in which the organic phase was the dispersed phase:

1. Data from four runs obtained with the system kerosene-water [axial diffusivities calculated from these data were reported earlier (*18*)].
2. Data from eight runs obtained with kerosene dispersed in an aqueous solution of potassium iodide; physical properties for this system are given in a footnote in Table 6.*

The θ, σ, and γ calculated from these two sets of drop residence time distribution curves are tabulated in Table 6.*

The values of standard deviation and skewness for the joint (rise time plus diffusion) distribution model and for the drop residence time distribution experiments are plotted in Figure 13. Also shown on this figure are the (dashed) $\gamma - \sigma$ curves that would be expected if the drop phase retention time characteristics were governed solely by eddy diffusion of drops of uniform size, or by flow of uniform drops through a series of perfectly mixed stages. For these latter cases the σ, γ relations are given by:

Eddy diffusion of uniform drops (reference *19*, case IV):

$$\sigma = \frac{1}{N_{Pe}}\sqrt{2N_{Pe} - 2\left(1 - e^{-N_{Pe}}\right)} \tag{22}$$

$$\gamma = \frac{2\sqrt[3]{3}}{N_{Pe}}\left[\frac{N_{Pe}}{2} - 1 + \left(\frac{N_{Pe}}{2} + 1\right)e^{-N_{Pe}}\right]^{1/3} \tag{23}$$

where $N_{Pe} = VL/E_b$

Series of well mixed stages:

$$\sigma = \frac{1}{\sqrt{n}} \tag{24}$$

$$\gamma = \sigma(2\sigma)^{1/3} \tag{25}$$

The information on Figure 13 shows that the skewness-variance relations for the joint model and for the tracer experiments are approximately the same, although the data for the joint model fall somewhat higher. One takes this to mean that the model, rise time plus eddy diffusion, is essentially the correct one to represent drop residence time distributions (for noninteracting drop systems), and that the differences between the model and the experiments are due to errors in the drop-counting technique, to the method used in extrapolating the curves to long times, to actual drop coalescence, or to other cause.

Secondly, Figure 13 shows that both the joint model and the experiments give skewnesses that are much greater than can be expected when eddy diffusion (of uniform drops) is the sole spreading process. This result might appear to indicate that the eddy diffusion mechanism imposed in the joint model is less important than are the drop size distribution parameters in determining the characteristics of the dispersed phase residence time curve. This is not always the case, however, especially for a high rotor speed [which results in small values of N_{PeDi} due to small u_{di} and large E_b, see Equations (18) and (19)]. The distribution curves for the joint model and for just the drop rise-time effect, already cited in Figure 11 for one run made at 1,100 rev./min., show that eddy diffusion makes a considerable contribution in this case.

* See footnote on p. 828.

MASS TRANSFER MODEL

This work and previous studies (*18*) indicate that the following departures from ideal flow behavior exist in an RDC of conventional design:

1. Eddy diffusion and axial diffusion of the continuous phase.
2. Eddy diffusion of the drop phase.
3. Distributions of drop sizes (areas), contact times, and rise velocities.
4. Drop interaction effects.

Undoubtedly the same phenomena exist in all contactors of the continuum or nondiscrete stage type; these include spray columns and rotating-impeller and rotating-cylinder contactors. Perforated plate columns and mixer-settler stages, which provide abrupt coalescence and redispersion at each stage, represent a special case. The mass transfer-eddy diffusion model based on uniform drops (*16, 18*) already brings in items 1 and 2. An outline of the transfer model that incorporates item 3 as well as 1 and 2 is given below. Item 4 cannot be included at this time, since information concerning probabilities of interaction of different size fractions in a drop population is not yet available.

For countercurrent flow and solute transfer between a continuous phase and a drop population of size distribution $f(d)$, the material balance equations over a differential slice of extractor are obtained by a solute balance on the drop fraction of diameters between d and $d + \delta d$, followed by integration over the size distribution. For the case of solvent phase continuous and feed phase dispersed, the set of equations plus boundary conditions are:

$$E_c \frac{d^2y}{dz^2} + \frac{V_c}{1-h}\frac{dy}{dz} = -\frac{6h}{1-h}\int_{d_o}^{d_m} \frac{K_D(d)}{d} f(d)\,[x(d) - my]\delta d \qquad (26)$$

$$E_D \frac{d^2}{dz^2}\int_{d_o}^{d_m} x(d)f(d)\delta d - \int_{d_o}^{d_m} u_d(d)f(d)\frac{d}{dz}[x(d)]\delta d = 6\int_{d_o}^{d_m}\frac{K_D(d)}{d} f(d)\,[x(d) - my]\delta d \qquad (27)$$

with

$$z = 0:\ \frac{dy}{dz} = 0 \qquad (28)$$

$$-E_D\frac{d}{dz}\int_{d_o}^{d_m} x(d)f(d)\delta d + \int_{d_o}^{d_m} u_d(d)f(d)\,[x(d) - x^o]\delta d = 0 \qquad (29)$$

$$z = L:\ E_c\frac{dy}{dz} + \frac{V_c}{1-h}(y - y^o) = 0 \qquad (30)$$

$$\frac{d}{dz}\int_{d_o}^{d_m} x(d)f(d)\delta d = 0 \qquad (31)$$

Here, $a = 6/d$ is used for the specific surface area of (spherical) drops in the interval d to $d + \delta d$. To avoid mathematical inconsistencies, a limit distribution [of the type proposed by Mugele (*11*), for example] would be used to represent the function $f(d)$, bounded by d_m and d_o in the two limits. Associated information needed in order to apply the above set of equations include drop dynamics relations [for example, Equations (2), (3), and (3*a*)] and a mechanism for mass transfer as a function of drop size.

The model has not yet been solved numerically because of the excessive number of calculations required to represent all parameter space. Nevertheless, certain situations that are general for any type of countercurrent extractor can be visualized wherein the model may be required, that is, cases where the uniform drop model may be significantly in error. As an aid in discussing these situations one may list the parameters that would be required to represent the solute recovery fraction for the i^{th} size fraction, according to the above model

$$\psi_i = \frac{x^o - x_i}{x^o - my^o} = fn\left(\frac{mQ_f}{Q_s}, \frac{6K_iL}{d_i u_{di}}, \frac{V_cL}{(1-h)E_c}, \frac{u_{di}L}{E_D}, f(d_i)\right) \qquad (32)$$

where

$$f(d_i) = fn(d_m, d_o, a, \delta) \qquad (33)$$

and the corresponding functional relation for the average recovery fraction based on the uniform drop model (*16*):

$$\bar{\psi} = \frac{x_o - \bar{x}}{x_o - my_o} = fn\left(\frac{mQ_f}{Q_s}, \frac{\overline{Ka}L}{V_D}, \frac{V_cL}{(1-h)E_c}, \frac{V_DL}{hE_D}\right) \qquad (34)$$

These relations reveal that:

1. The recovery fraction based on the uniform drop model will probably differ the most from that for the size distribution model when molecular diffusion in the drops controls mass transfer [Equation (5), $K \sim d^{-1}$], will differ the least when circulating-oscillating drop transfer dominates ($K \sim u$), and will differ to an intermediate degree when a surface renewal or equivalent mechanism dominates transfer ($K \sim \sqrt{u/d}$).
2. If backmixing is indicated to be severe for the uniform-drop case (small values of N_{Pec} and N_{PeD}), then $u_{di}L/E_D$ will be still smaller for a substantial fraction of the small drops present. Therefore, the extraction efficiency for this fraction may be poor even though the contact time (L/u_{di}) is long.
3. The K_ia_i and L/u_{di} for the fraction of largest drops may be such that ψ_i for this fraction is substantially less than the average ψ based on uniform-drop calculations. In such event it may be impossible to achieve the desired average rejection ($1 - \bar{\psi}$) in the given column length, even though extraction is essentially complete for all drops smaller than the average drop.

The uniform drop model may, in fact, be used to investigate some limiting conditions when a drop size distribution is present. Such calculations supply guidance in the selection of a safety factor to be used with that model. As an example, and one that illustrates item (3) above, calculations with the Sleicher (*16*) solution and based on average drop properties show that $\bar{\psi} = 0.982$ when $T = 10$, $F = 0.25$, and N_{Pec} and $N_{PeD} = 10$. But for a typical size distribution, 10% volume of the drops may have a d_i that is twice d_{32}. For this fraction $(N_{PeD})_i \cong 20$, but T_i may be only about 2.5 (since a_i decreases and u_{di} increases, relative to the average drop), for these values one calculates $\psi_i \cong 0.824$ from the Sleicher relations. This means that $\bar{\psi} = 0.982$ cannot be achieved at the given design conditions since ~100% extraction is then required for the other 90% of the drops. Some increase in column length or a decrease in drop size across the whole distribution is required in order to increase the T_i's for the larger drops.

DISCUSSION

This work provides a further demonstration of the existence of a fairly wide distribution of drop sizes in a flow

contactor and is therefore complementary to the findings of numerous other investigators (*1, 6, 7, 13, 14, 15*) who have worked with various types of equipment. The fact that such distributions do exist in most types of mass transfer apparatus simply means that a mass transfer mechanism based on uniform-drop assumptions is not a very elegant means for interpreting such data. The interpretations and observations given here represent only a first step in the direction of putting such calculations on a more rigorous basis.

Various interesting and useful areas for further study are nonetheless delineated. These include a description of the break-up process, with common disperser devices, that explains the formation of a wide size distribution; whether such distributions are changed by typical drop interaction processes in a flow environment (which, of necessity, must include interaction rates between drops of unequal size); and an elucidation of axial mixing and mass transfer processes for a drop population in flow apparatus.

ACKNOWLEDGMENT

The author wishes to acknowledge the assistance and suggestions of G. H. Ackerman and C. P. Strand, and the specific suggestions of L. B. Rothfeld as to the essential features of Equations (26) through (31).

NOTATION

a = surface area per unit volume; skewness parameter, upper limit distribution
A_c = area of drop photograph counted; A_t = total area of photograph
b_0, b_1 = constants in Equation (17)
C = concentration or frequency factor, Equation (20)
C_R = constriction factor, Equation (4)
d = drop size; $\overline{d}$ = characteristic average size; d_m = d_{max} = maximum stable drop size; d_o = d_{min} = minimum drop size; d_{32} = volume surface mean size; d_{95}, d_{50}, d_{10}, d_5 = drop sizes corresponding to 95, 50, 10, and 5% of the cumulative distribution
D = column diameter
$\mathcal{D}_c$ = molecular diffusivity in continuous phase; $\mathcal{D}_D$ = same, drop phase
E_b = eddy diffusivity; E_c = effective diffusivity, continuous phase; E_D = effective diffusivity, dispersed phase
f = volume fraction of drops of a given size, as seen by observer; drop size distribution function
F = mQ_f/Q_s = extraction factor
g = volume fraction of drops of a given size, originating from feed
h = volume fraction holdup of dispersed phase
H = compartment height
k_c = individual transfer coefficient, continuous phase; k_D = same, dispersed phase
K = overall transfer coefficient
L = column length or length of test section
m = distribution coefficient
n = number of drops; number of mixed stages in series
n_m = number of maximum stable drops on photograph
N = rotor speed
N_{Pe} = Peclet number, N_{Pec} = same, continuous phase; N_{PeD} = same, dispersed phase
p = probability; number of size fractions; p_o = normalization factor
Q_f = volume flow rate, feed phase; Q_s = same, solvent phase
R = rotor diameter
S = stator opening
t = time; $\overline{t}$ = rise time of drops of size $\overline{d}$
T = number of transfer units; $\overline{T}$ = average transfer units for drop population
u = slip velocity; $\overline{u}$ = slip velocity of drops of size $\overline{d}$
u_d = drop velocity, defined by Equation (3*a*); u_{dm}, u_{d90}, u_{d50}, u_{d10} = drop velocities corresponding to d_m, d_{90}, d_{50}, d_{10}, etc.
v = volume of drops, Equation (7); dummy time variable, Equations (20) and (21)
V = superficial velocity; V_c = same, continuous phase; V_D = same, dispersed phase
x = solute concentration in drop (feed) phase; x^o = same, in entering feed
y = variable defined by Equation (8); solute concentration in continuous (solvent) phase; y^o = same, in entering solvent
z = length variable
Z = geometry function, Equation (12)

Greek Letters

γ = relative skewness
δ = uniformity parameter, upper limit distribution
θ = average residence time
λ = dimensionless time variable, Equation (20)
μ_c = viscosity, continuous phase; μ_D = same, dispersed phase
ρ_c = density, continuous phase; ρ_D = same, dispersed phase; $\overline{\rho}$ = average density of two-phase mixture
σ = interfacial tension; relative standard deviation
ψ = recovery fraction, Equation (32); $\overline{\psi}$ = average recovery fraction for entire drop population

Subscripts

i = fraction of drops of size d_i
n = n^{th} time increment

LITERATURE CITED

1. Clay, P. H., *Nad. Akad. van Wetenskapen Proc.*, **43**, 852, 979 (1940).
2. Handlos, A. E., and Thomas Baron, *A.I.Ch.E. Journal*, **3**, 127 (1957).
3. Hinze, J. O., *ibid.*, **1**, 289 (1955).
4. Hu, Shengen, and R. C. Kintner, *ibid.*, p. 43.
5. Hughes, R. R., and E. R. Gilliland, *Chem. Eng. Progr.*, **48**, 497 (1952).
6. Huttig, G. F., and H. Stadler, *Monatsch.*, **88**, 150 (1957).
7. Keith, F. W., and A. N. Hixson, *Ind. Eng. Chem.*, **47**, 258 (1955).
8. Licht, William, and G. S. R. Narasimhamurty, *A.I.Ch.E. Journal*, **1**, 366 (1955).
9. Madden, A. J., and G. L. Damerell, *ibid.*, **8**, 233 (1962).
10. Miller, R. S., J. L. Ralph, R. L. Curl, and G. D. Towell, *ibid.*, **9**, 196 (1963).
11. Mugele, R. A., and H. D. Evans, *Ind. Eng. Chem.*, **43**, 1317 (1951).
12. ———, *A.I.Ch.E. Journal*, **6**, 3 (1960).
13. Nagata, S., and I. Yamaguchi, *Mem. Fac. Eng. Kyoto Univ.*, **22**, Pt. 2, p. 249 (1960).
14. Rodger, W. A., V. G. Trice, and J. H. Rushton, *Chem. Eng. Progr.*, **52**, 515 (1956).
15. Scott, L. S., W. B. Hayes, and C. D. Holland, *A.I.Ch.E. Journal*, **4**, 346 (1958).
16. Sleicher, C. A., Jr., *ibid.*, **5**, 145 (1959).
17. *Ibid.*, **8**, 471 (1962).
18. Strand, C. P., R. B. Olney, and G. H. Ackerman, *A.I.Ch.E. Journal*, **8**, 252 (1962).
19. van der Laan, E. T., *Chem. Eng. Sci.*, **7**, 187 (1958).

Manuscript received January 27, 1964; revision received May 13, 1964; paper accepted May 14, 1964. Paper presented at A.I.Ch.E. Pittsburgh meeting.